SI Appendix for "Coal fly ash is a major carbon flux in the Chang Jiang (Yangtze River) basin"

by Li et al.

Contents

S1. Sample collection

To characterize organic carbon in the Chang Jiang (Yangtze River) basin, we collected a comprehensive set of samples from fly ash, shale, river sediment, Holocene sediment, and standing biomass. All sample information is compiled in Appendix Table S1. In summary, the fly ash samples were collected from wasted coal ash piles from several coal-fired power plants, a coking plant, and an aluminum plant in east China, and from a coal ash pile aside a boiler-heater unit in the campus of Nanjing University, China. Fresh shale samples were collected from sedimentary sequences in the lower-middle CJ reach, nearby the cities of Nanjing, Chaohu, and Yichang, and the profiles were excavated during sampling to remove the surface weathered layers. Plant leaf samples were collected in the campus of Nanjing University. The Holocene core sediment samples were taken from the CM 97 core drilled at the Chongming Island at the Chang Jiang estuary, which were identified as deltaic, estuarine, fluvial and floodplain sedimentary facies (1). The Chang Jiang river suspended sediment samples were collected monthly from August 2007 to September 2008 in the lower reach near Nanjing, covering a complete hydrological year. Sampling details and results for the river suspended sediments were presented in a prior study (2). All sediment samples were dried at 40°C in the oven and grounded using an agate pestle and mortar.

S2. Laboratory analyses

Decarbonation and bulk OC measurement

The Holocene core sediment, shale, and fly ash samples were decarbonated using 5 M HCl at 75 °C to remove detrital carbonates following a previous work studying OC in river sediments in the Andes (3). Bulk OC content was measured on decarbonated samples using an element analyzer. Samples were weighed before and after decarbonation to correct for the OC content in raw samples.

Chemical oxidation

We conducted oxidation experiments following the protocol described in ref.(4). In summary, a solid sample of 0.5 g was put in 250 mL DI water and the mixture was sonicated. Then, 20 g Na_2S_2O8 and 22 g $NaHCO_3$ (as buffering agent) were added to the solution. The oxidation experiment was conducted at 80 °C for 48 hours on a heater equipped with a magnetic stirrer. After oxidation, the sample was treated with 20 mL 0.01 M HCl and 20 mL DI water to remove any trace carbonate produced during oxidation. The sample was then washed with DI water to neutralize pH, and dried in the oven.

Raman spectral analysis

To characterize the structure of OC in the samples, Raman spectral analysis was performed on raw samples using a Renishaw RM2000 Raman spectrometer in the School of Earth Sciences and Engineering at Nanjing University, China. We adopted a synchrosan band mode 100 cm^{-1} to 2000 cm^{-1} to capture the bands for inorganic minerals (200-1100 cm^{-1}) and carbonaceous matter (1300-1600 cm^{-1}) (Fig. S2), with the other configuration parameters set as suggested in an earlier study of OC in the Himalayan river systems (5). The position of a standard silicon wafer was repeatedly measured for calibration.

We decomposed the carbonaceous band into G and D bands (Figs. S2-S3), which correspond to graphite and defects, respectively (5, 6). Following a prior study (6), we resolved the carbonaceous material band as G band and D1, D2, D3, and D4 bands by fitting Lorentzian profiles to five Raman peaks (Fig. S3).

Ramped pyrolysis oxidation (RPO) analysis

Ramped pyrolysis oxidation analysis was done on a shale sample and a fly ash sample using the instrumentation at the National Ocean Sciences Accelerator Mass Spectrometry (NOSAMS) facility. Technical details and workflow were described in previous studies (7-9). In brief, a solid sample containing around 100-300 µg carbon was loaded into a pre-heated quartz reactor in an oven. The oven was programmed to heat at a ramp rate of 20 °C min^{-1}, from ambient temperature to 1000 °C. The experiment was done under the oxidation mode using carrier gas composed of 98% He and 2% O_2 and with a gas flow rate of 35 mL min^{-1}. As the sample was heated and oxidized, the eluent gas was sent into an infrared gas analyzer where CO_2 concentration was measured at 1 s temporal resolution. As a result, a thermogram was obtained showing the evolution of the monitored CO_2 concentration over time and temperature. To characterize OC reactivity and bond strength, we converted the obtained thermograms to the activation energy (E_a) spectra using the 'rampedpyrox' Python package developed by Hemingway et al. (8) (code available from the GitHub repository at https://github.com/FluvialSeds/rampedpyrox), which implemented an inverse model to find the optimal solution of a set of parallel first-order kinetic decay reactions.

S3. Sources for data compilation and synthesis

Coal consumption

The coal consumption data in China from 1950-2010 was adopted from Table 7-2 in China Statistical Yearbook (1999, 2012) by the National Bureau of Statistics of China (NBSC) (http://www.stats.gov.cn/tjsj/ndsj/, http://www.stats.gov.cn/yearbook/indexC.htm) (10, 11)

Fly ash production and utilization

The fly ash production and utilization data were adopted from Yao et al. (12) and references therein. Specifically, the fly ash data in China were obtained from the *Annual Report on Comprehensive Utilization of Resources of China* released by the National Development and Reform Commission of the People's Republic of China (http://www.gov.cn/gzdt/2013-04/08/content_2372577.htm) (13). China fly ash data were only available from 2001 to 2015 (12). To validate the coal and fly ash data, we use the two datasets to calculate an average fly ash content in coal by linearly regressing the two datasets with a defined Y-intercept of 0 (Fig. S1). Thus we estimate an average fly ash content of 17%

for coal consumed in China, well within the normal range of fly ash content in coals of 5-20% (12).

To quantify fly ash production in years prior to 2001 when fly ash data is not available but coal consumption data is available, we multiply the coal consumption in those years by our calculated average fly ash content of 17% in 2001-2015 (Fig. S1). This approach likely provides a lower estimate as the ash content is expected to have decreased over time with improvement in combustion efficiency and coal cleaning (Fig. S1d).

To determine the total fly ash production in the CJ basin, we summed coal consumption in all provinces within the CJ basin and calculated the ratio between coal consumption in the CJ basin and the national total consumption, from 1990 to 2011 (Table 4-15 in China Energy Statistical Yearbook, 2012, by the National Bureau of Statistics of the People's Republic of China) (14). We find an average value of 36.3±0.1% (1990-2011) as the fraction of coal consumed in the CJ basin versus in the whole country.

To estimate how much fly ash is wasted rather than utilized (Fig. 3c), we calculate the difference between the totally produced fly ash and utilized fly ash. The utilized part is determined as the product of the total production and utilization rate. The utilization data is available from 2001 to 2015 with an increase in proportion of total coal combustion from 62% to 70%, as compiled by Yao et al. (12) from the reports from the National Development and Reform Commission of the People's Republic of China (12). For years prior to 2001, we adopt a utilization proportion of 62% as of 2001, and recognize that actual utilization would be lower (wasted ash would be higher) considering a general growing trend over time (12). Thus our calculations of fly ash production and release in the CJ basin provide a lower and conservative estimate.

Chang Jiang suspended sediment flux

The Chang Jiang sediment flux data for year when samples were collected (2007-2008) was adopted from the Chang Jiang Sediment Bulletin (2009) (http://www.cjw.gov.cn/zwzc/bmgb/2018gb/) (15) at the Datong station in the lower CJ reach, as determined from hydrological gauging. The annual CJ sediment flux data during 1950-2000s was compiled in ref. (16).

Coal fire power plant

The map of coal-fired power plants in east and central China (Fig. 1b) is based on multiple databases including the *Global Coal Plant Tracker* database (Global Energy Monitor, 2019, https://endcoal.org/global-coal-plant-tracker/, https://www.carbonbrief.org/mapped-worlds-coal-power-plants) (17), and the *Carbon Dioxide Emissions From Power Plants Worldwide* (CARMA) database (https://www.cgdev.org/article/carma-v30-reveals-new-data-co2-emissions-corporate-ownership-and-locations-60000-power) (18). We use this map to show the general regional pattern, with coal-fired power plants clustered in the middle-lower Chang Jiang basin. These provide a major source of fly ash and FOC_{ash}. However, we do not use the map to conduct any quantitative calculations because the databases may not be complete in documenting fly ash sources.

Large reservoir data

The map of large reservoirs (with capacity > 0.1 km^3) in the Chang Jiang River basin was made from multiple sources including ref. (19), the 'Database of the Basic Characteristics of Chinese Large and Medium-Scale Reservoirs' by the Inland Water Biological Division of Chinese Biodiversity Information Center (https://web.archive.org/web/20120330041630/http://brim.ihb.ac.cn/indexen.aspx) (20), and a database, *Code for China Reservoir Name*, compiled by the Ministry of Water Resources, People's Republic of China (2011) (21), with reference to the satellite images on Google Earth.

S4. End-member mixing model in the oxidation fraction (f_{ox})-1/OC space

Here we derive the mixing model used to distinguish the contributions of different components to the riverine OC, with results presented in the main text (additional mixing trends used to constrain the model are shown in Fig. 2d and SI Appendix Fig. S2). Riverine-carried particulate OC is a mixture of OC sourced from biosphere (OC_{bio}) and lithosphere (OC_{fossil}) (22, 23), which can be expressed based on the mass balance of concentrations within a given sediment sample:

$$[OC] = [OC]_{bio} + [OC]_{fossil} \quad \text{(Eq. S1)}$$

During the oxidation experiment, the oxidized carbon, $[OC]_{ox}$, is composed of oxidized OC_{bio} and oxidized OC_{fossil}, so we can write:

$$[OC]_{ox} = [OC]_{bio\text{-}ox} + [OC]_{fossil\text{-}ox} \quad \text{(Eq. S2)}$$

where the subscripts ox, bio-ox, and fossil-ox mean total oxidized carbon, oxidized biospheric OC, and oxidized fossil OC, respectively.

For bulk OC in river sediments, we use an oxidation fraction (f_{ox}) to quantify OC loss during oxidation experiments.

$$[OC]_{ox} = f_{ox} \times [OC] \quad \text{(Eq. S3)}$$

We then define an analogous oxidation fraction for OC_{bio}, $f_{ox\text{-}bio}$, which gives:

$$[OC]_{bio\text{-}ox} = f_{ox\text{-}bio} \times [OC]_{bio} \quad \text{(Eq. S4)}$$

Similarly, we define an oxidation fraction for OC_{fossil}, $f_{ox\text{-}fossil}$:

$$[OC]_{fossil\text{-}ox} = f_{ox\text{-}fossil} \times [OC]_{fossil} \quad \text{(Eq. S5)}$$

Combining Equations S2-S5, we have:

$$f_{ox} \times [OC] = f_{ox\text{-}bio} \times [OC]_{bio} + f_{ox\text{-}fossil} \times [OC]_{fossil} \quad \text{(Eq. S6)}$$

We rewrite Eq. S6, yielding:

$$f_{ox} = f_{ox\text{-}bio} \times [OC]_{bio}/[OC] + f_{ox\text{-}fossil} \times [OC]_{fossil}/[OC] \quad \text{(Eq. S7)}$$

A prior study (2) showed that in the Chang Jiang river sediment, $f_{ox\text{-}fossil} = 0$, which is expected because after substantial remineralization and oxidation of fossil OC during erosion and fluvial transfer (5, 24-26), only the most refractory component can be preserved in the river sediment. Taking this observation into Eq. S7 gives:

$$f_{ox} = f_{ox\text{-}bio} \times [OC]_{bio}/[OC] \quad \text{(Eq. S8)}$$

As $[OC]_{bio} = [OC] - [OC]_{fossil}$ (Eq. S1), we have:

$$f_{ox} = f_{ox\text{-}bio} \times ([OC] - [OC]_{fossil})/[OC] \quad \text{(Eq. S9)}$$

Letting $f_{ox} = Y$, and $1/[OC] = X$, then:

$$Y = f_{ox\text{-}bio} - f_{ox\text{-}bio} \times [OC]_{fossil} \times X \quad \text{(Eq. S10)}$$

Thus, Equation S10 demonstrates a linear relationship between f_{ox} and 1/[OC], where the intercept at the X-axis is $[OC]_{fossil}$, the intercept at the Y-axis is $f_{ox\text{-}bio}$, and the slope is their product, $f_{ox\text{-}bio} \times [OC]_{fossil}$ (Figs. 2d, 2e and S2). By fitting lines to the observed data, we can determine these unknown parameters.

S5. Flux estimate and error propagation

We use two primary approaches to determine the fraction of fly ash-sourced fossil OC in the Chang Jiang-exported fossil OC ($f_{FOC\text{-}ash}$).

Mass balance approach

We conduct a mass balance calculation between FOC_{ash} and FOC in ash-uncontaminated river sediment (FOC_{CJ0}), as:

$$[FOC]_{ash} \times (f_{sed\text{-}ash}) + [FOC]_{CJ0} \times (1 - f_{sed\text{-}ash}) = [FOC]_{CJ} \quad \text{(Eq. S11)}$$

where $f_{sed\text{-}ash}$ is the mass fraction of fly ash in the CJ sediment flux, and $[FOC]_{CJ}$ is the apparent content of FOC in the CJ sediment (0.45±0.10%) determined from radiocarbon measurements (2). $[FOC]_{CJ0}$ is 0.15±0.02% from the oxidation experiment.

The fraction of FOC_{ash} in the CJ-exported FOC is calculated as:

$$f_{FOC\text{-}ash} = [FOC]_{ash} \times (f_{sed\text{-}ash}) / [FOC]_{CJ} \quad \text{(Eq. S12)}$$

And the riverine FOC_{ash} flux is calculated as:

$$Q_{FOC\text{-}ash} = [FOC]_{ash} \times (f_{sed\text{-}ash}) \times Q_{sed} \quad \text{(Eq. S13)}$$

where Q_{sed} is the total sediment flux (~130 Mt yr^{-1} in the sampling year) (15, 27).

To propagate errors on $f_{sed\text{-}ash}$, $f_{FOC\text{-}ash}$, and $Q_{FOC\text{-}ash}$, we conduct Monte Carlo random sampling calculations. In each iteration, we randomly sample $[FOC]_{ash}$ following the probability distribution of the measured histogram of $[FOC]_{ash}$, sample $[FOC]_{CJ0}$ and $[FOC]_{CJ}$ following two normal distributions of 0.15±0.02% (this study) and 0.45±0.10% (2) (mean ± 1σ), respectively, and solve Equations S11-S13 simultaneously. We conduct 10,000 iterations and generate a population of results. We report the median values and define the uncertainties from the 16^{th}-84^{th} percentiles of the resulted population. We also use this approach to estimate the errors on the fraction of riverine-carried fly ash in the totally produced fly ash and in the wasted (produced – utilized) fly ash in the CJ basin.

Constraint from magnetic susceptibility (MS) study (28)

We refer to an independent study that observed increases in MS of CJ sediment and attributed these changes to input of fly ash (28). They estimate a $f_{sed\text{-}ash}$ of 7% on this basis. Taking this value into Equations S11-S13, we can estimate $f_{FOC\text{-}ash}$ and $Q_{FOC\text{-}ash}$, respectively, and propagate the errors using the same Monte Carlo random sampling approach.

S6. Expanded discussion on FOC_{ash}: origins, forms, separation, and controlling factors

FOC_{ash} is also termed 'unburned carbon'. Major research efforts have been devoted to imaging, characterizing, separating, and recovering or removing FOC_{ash}. Referring to recent studies (29-34) and review papers (35-39) on FOC_{ash}, below we summarized (1) the industrial standards for FOC_{ash} content, (2) the identification and classification of different carbon species in FOC_{ash}, (3) the separation methods of FOC_{ash}, and (4) the controlling factors of FOC_{ash}, to complement the discussion of the characteristics of FOC_{ash} in the main text.

Industrial standards of FOC_{ash} content

FOC_{ash} provides a measure for the efficiency of combustion (39, 40). When utilizing fly ash as concrete, air entraining agents are added to fly ash to improve air entrainment performance, but are easily absorbed by FOC_{ash} (39-42). Thus FOC_{ash} amounts need to be controlled for ash quality assurance (34, 35, 39). As a result, industrial standards of FOC_{ash} contents have been established. Dong et al. (34) compiled the industrial standards of FOC_{ash} content in different regions and countries, finding that these are consistently around 5-10%. We list here the standards for FOC_{ash} contents for major coal-consumption countries and regions. The US ASTM-C618 standard states that for class-F (from anthracite and bituminous coal, siliceous with <10% CaO by mass) and class-C (from subbituminous and lignite coal, containing mainly lime with 10-40% CaO) fly ash, loss on

ignition (LOI, as an approximation for FOC_{ash}) needs to be within 6% if using ash for construction materials (34, 37, 43). The Chinese national standard GB/T477-2008 for fly ash used in cement and concrete states that LOI needs to be within 5% and 8% for grade I and II fly ash, respectively (34, 35). In Europe, the EU standard EN 450 states that LOI should be within 5%, 2-7%, and 4-9% for category A, B, and C fly ash, respectively, for use in concrete and cement (34, 44). The Australian standard AS3852.1 recommends LOI within 4% for use in concrete (37, 45). The Indian standard 3812 states a upper limit of LOI as 5% (34, 44). The Russian standard GOST 25818 has permitted limits of 20%, 10%, and 3% for type I fly ash for anthracite coal, hard coal, and brown coal, respectively (34, 46).

Classification of carbon species in FOC_{ash}

FOC_{ash} contains a spectrum of carbon species with varying compositions, sizes, origins, structures, and relationships with minerals. Here we introduced the major methods employed to classify FOC_{ash} to facilitate intercomparison.

Considering elemental composition, FOC_{ash} can be classified as elemental carbon (EC) and organic carbon (OC) (29, 30, 35). EC is mainly graphite or graphitic carbon, whereas OC is carbon bonded to other atoms such as hydrogen and oxygen (29, 30).

Observational studies based on scanning electron microscopy (SEM) and high-resolution transmission electron microscopy (HRTEM) indicated that FOC_{ash} is composed of two major carbon forms: individual carbon particles and mineral-associated carbon (31, 35, 37, 41, 47). The carbon particles include (1) monomer char particles from incomplete combustion featured by irregular shapes with sizes of 1s-10s μm (37, 47, 48), and (2) aggregates of fine carbon particles (1s-10s nm) that are likely sourced from soot (37, 42, 48, 49). The mineral-associated carbon contains (1) carbon attached to mineral surfaces, and (2) carbon embedded in minerals as inclusions (35, 47).

Other studies combined the sizes and characteristics of different carbon species in FOC_{ash} to infer their sources and origins. Specifically, soot-sourced carbon tends to cluster as spherical particles, in the size range of ones to tens of nm, that can attach to the surfaces of and aggregate in the structures of minerals and char particles (ones to tens of μm), and form aggregates themselves (37, 42, 48, 49). Char particles, from the incomplete combustion of coal, have irregular shapes and highly porous structures (37, 47, 48). Mineral-associated carbon can contain inherited carbon that has fine sizes from incomplete combustion of coal (e.g. the inertinite maceral), thermally altered carbon during combustion, and carbon from other origins (e.g. soot) that later form associations with ash particles (30, 37, 38, 50).

Overall, these are the different carbon species that compose FOC_{ash} , and thus we accounted for these in our budget calculations. These forms of carbon may still have have variable reactivity (e.g. graphitic carbon vs. non-graphitic carbon), but are expected to be substantially recalcitrant, as evidenced by our chemical oxidation experiments and the dominance of graphitic structures and mineral associations which are effective mechanisms for carbon preservation (7, 51).

Separation of FOC_{ash}

Significant research efforts have been devoted to separating the unburned carbon species from fly ash to improve the efficiency of ash utilization. Several studies summarized the major approaches used for separating FOC_{ash} including size separation, gravity separation, electrostatic separation, froth flotation and oil agglomeration, and thermal processing (35, 52). Here we described the major separation methods in brief, with reference to recent review papers and relevant studies (35, 37, 52), to complement our discussion of the characteristics of FOC_{ash}. The separation methods listed below were developed based on characteristics of FOC_{ash} including its size, gravity, structure, morphology, pore sizes, and charge property, and different methods have different ways of separating the carbon species.

Size separation, including both dry and wet sieving, is a simple and economical method to separate and recover unburned carbon from fly ash. Size separation through sieving is most effective for fly ash within which FOC_{ash} is dominated by coarse, unburned particles such as char, but cannot separate carbon species of finer sizes (e.g. soot carbon attached to ash particles) (35). This method is often used as a first step to screen fly ash before more advanced processing (e.g. electrostatic separation) (53).

Gravity separation is based on the density differences between FOC_{ash} and fly ash minerals (35). Laboratory experiments showed that gravity separation combined with other techniques such as centrifuging and triboelectrostatic enrichment can work effectively to remove unburned carbon (e.g. >80%) for the coarse fraction of fly ash (54).

Thermal treatment is another commercially used approach to remove unburned carbon from fly ash (37). One commonly used equipment is fluidized-bed reactors, which can combust fly ash in a continuous stream (55). Fluidized-bed reactors can recycle burned fly ash with high carbon content to maintain bed temperature and reduce consumption of supplemental fuel (55). This technique has no requirement on the freshness of fly ash and can be used to process long-disposed ash as well (37).

More advanced separation methods include electrostatic separation, froth flotation, and oil agglomeration, which have been widely used in oil and mining industry (35, 48, 52, 54). Electrostatic separation takes advantage of the charge property of FOC_{ash}: ash particles and unburned carbon have distinct electron affinities, such that during charging, fly ash particles tend to gain electrons and becoming negatively charged, whereas unburned carbon more easily loses electrons to be positively charged (35, 49, 56). This method charges fly ash and carbon particles, and once charged, the charged fly ash and unburned carbon particles are delivered to a high-voltage electrostatic field where the particles carrying distinct charges and polarities are deflected and separated (35, 55, 57). Combining different charging mechanisms (e.g. triboelectric charging and induction charging) and equipment (e.g. drum separator, triboelectric belt separator, and parallel and louvered plate separators), electrostatic separation can be applied to both coarse- and fine-sized (e.g. < 1 μm) fly ash (56). Drying is a common procedure when preparing ash for electrostatic separation, because moisture decreases the efficiency of electrostatic separation (57).

Froth flotation is a widely used technique in coal and mining industry to separate materials based on their hydrophobicity (58-60), and has been used to separate the hydrophobic unburned carbon and the hydrophilic ash minerals as well (35, 48, 61-63). In froth flotation, fly ash is mixed with a surfactant (e.g. polar reagents) and water, and is delivered to a tank (i.e. flotation cell) where air is introduced and bubbles are generated (48, 59, 60). The hydrophobic carbon particles attach to the bubbles and float to the surface forming a froth, whereas the hydrophilic ash minerals remain in the solution and can be separated. Recent studies have focused on improving and developing flotation devices (e.g. Denver flotation cell, cyclonic-static microbubble flotation column, and concurrent flotation column) and testing different reagents (e.g. diesel oil and acetic acid) to increase the efficiency of bubble generation and particle separation (63-67). However, very fine carbon particles collide less frequently with bubbles, and thus cannot be effectively separated using froth flotation (35, 60, 62). Oil agglomeration complements froth flotation by separating unburned carbon from fine-sized fly ash (68, 69). In brief, fly ash is wetted by oil such that the hydrophobic, unburned carbon particles are coated with oil and form agglomerates, whereas the hydrophilic, ash mineral particles do not agglomerate and remain in suspension, with a recovery rate of unburned carbon as high as ~50-60% (53, 69).

We note that although the above methods can separate FOC_{ash}, none of them can quantitatively recover all carbon species from fly ash. Each method has its limitations and preferable carbon species in FOC_{ash} that can be recovered. For example, the froth flotation method works more effectively for carbon attached to mineral surfaces. Removing carbon aggregated in mineral structures often requires grinding and other methods to dissociate mineral and carbon (35, 52, 54).

Controlling factors of FOC_{ash}

A large number of studies have focused on understanding the factors determining the amount and forms of FOC_{ash}. Several reviews, notably Hower et al. (37), have summarized those factors comprehensively, and so here we briefly introduce those factors. In general, the controlling factors are related to (1) the nature of coal and (2) the design, configuration, and condition/operation of the combustion systems (35, 37, 41, 70, 71). Modeling studies also show that the FOC_{ash} content can be predicted using these two variables (32, 40).

The factors describing the nature of coal include coal rank, sizes, maceral composition, mineralogical composition, volatile content, moisture, and calorific value (32, 37, 40). Notably, it has been shown that decreasing particle size of the feed coal can increase combustion efficiency and reduce the FOC_{ash} content (72, 73). The abundances of different types of macerals (e.g. inertinite, vitrinite, and liptinite) that make up coal influence FOC_{ash} contents as well, whereby the inertinite macerals are more resistant during combustion than vitrinite macerals (74-77). Fly ash from coals with high proportions of intertinite macerals tend to have high FOC_{ash} amount (74-77). Hower et al. (37) showed in detail that coal rank plays a key role regulating the forms of FOC_{ash} as well. In summary, the fly ash produced from low-rank (lignite and subbituminous) coal contains FOC_{ash} of intact inertinite-derived carbon, thermally-altered vitrinite-sourced carbon, and isotropic char (37, 78, 79). FOC_{ash} produced from medium-rank (bituminous) coal mainly contains unaltered inertinite-sourced carbon, mixtures of isotropic and anisotropic coke originated from vitrinite, and amorphous and crystalline carbon in association with minerals (49, 80-84). The fly ash produced from high-rank

(anthracite) coal inherits carbon from the coal macerals experiencing limited alteration during combustion (85, 86).

The factors related to the combustion system include combustion time, coal feeding rate, damper position, burner tilt, coal-oxygen-air ratios, temperature and pressure in combustion systems, heat flow rates, and flame patterns (32, 37, 40).

S7. Compilation of FOC_{ash} content data in global fly ash samples

We compiled 247 FOC_{ash} content data from previous studies to constrain the amount of unburned carbon in fly ash worldwide (Table S2) (30, 33, 40-42, 47, 48, 50, 52, 71, 87-96). Those data were measured for fly ash samples from Australia, China, Canada, Spain, South Korea, South Africa, and the US (Table S2). Most samples were industrial coal fly ash collected from power stations, with a small fraction from fly ash produced from simulated combustion in laboratories. The FOC_{ash} contents were estimated either by loss on ignition (n = 212) or by ultimate analysis (i.e. elemental analysis) (n = 35) (30, 33, 40-42, 47, 48, 50, 52, 71, 87-96). The compiled FOC_{ash} contents likely overestimated the actual FOC_{ash} contents, because loss on ignition (LOI) measures mass loss once burned to high temperature (e.g. 950 °C, ASTM-Standard D7348, 2013) (37, 97) without excluding non-carbon elements and volatiles, and elemental analysis does not separate inorganic carbon (e.g. carbonate) (89, 90). The compiled FOC_{ash} contents show a skewed distribution with a median of 4.70% (1.30-14.39%, 16^{th}-84^{th} percentiles) and a majority of data within 10%. Note that the compiled FOC_{ash} content is comparable to the worldwide industrial standards of unburned carbon content in coal ash (5-10%, Appendix S6) (34) and our measured FOC_{ash} content in the CJ ash samples ($2.25^{+1.63}/_{-1.18}$%), lending confidence to our estimates of FOC_{ash} fluxes.

Supporting Information Appendix Figures

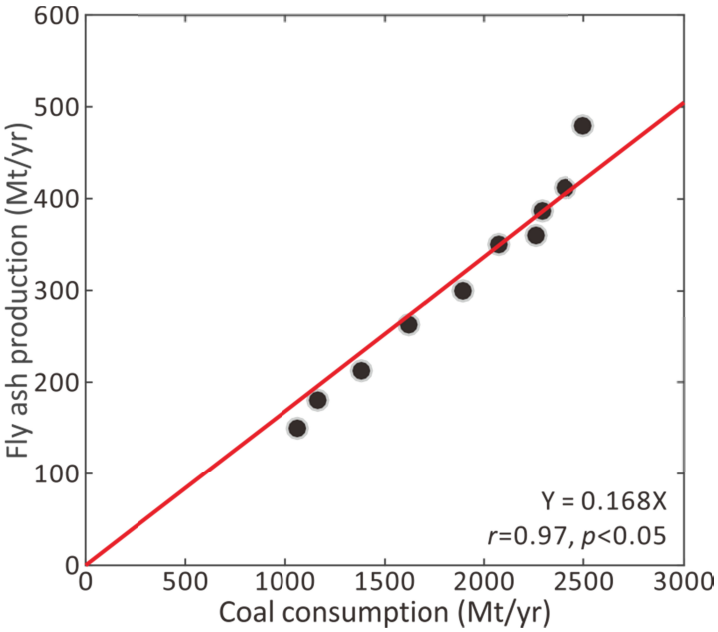

Figure S1. Relationship between coal consumption rate and fly ash production rate in China.

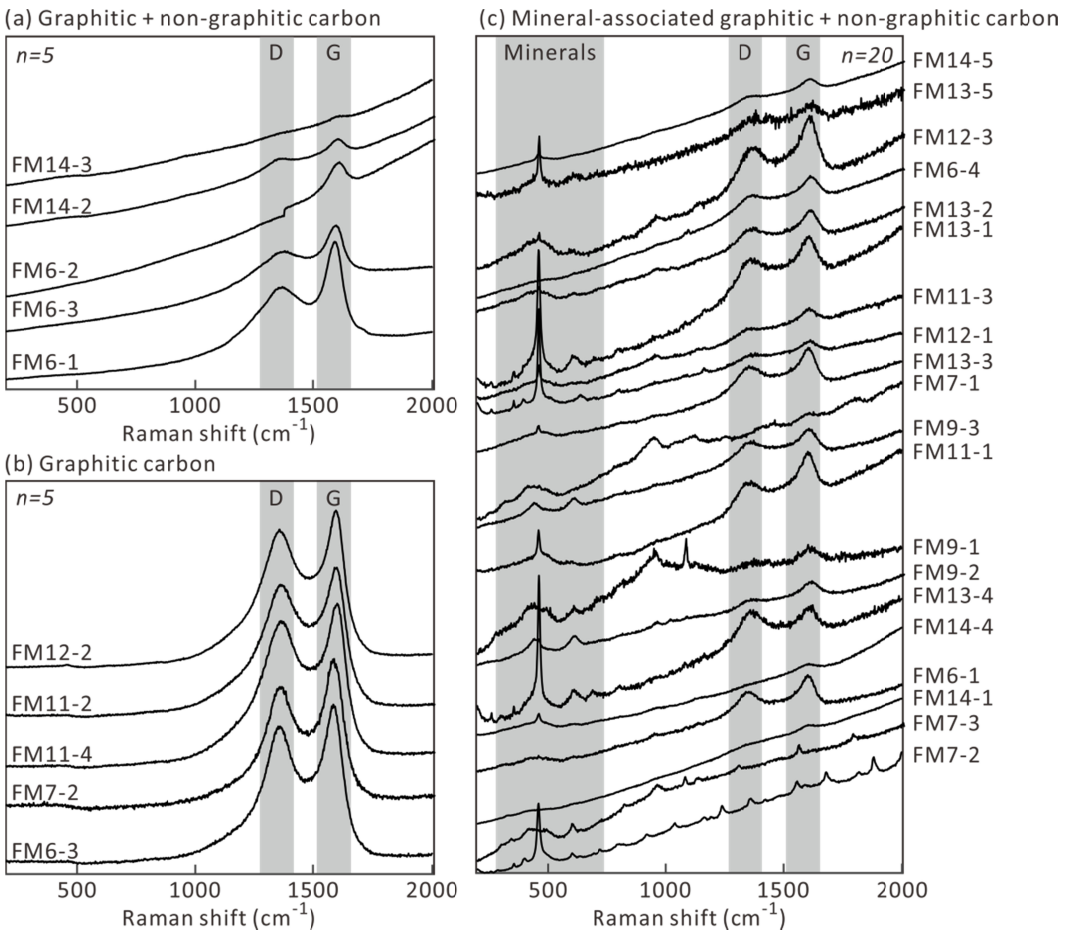

Figure S2. Raman spectra (raw data without baseline correction) of the CJ fly ash samples with FOC_{ash} as (a) mixtures of graphitic and non-graphitic carbon, (b) graphitic carbon, and (c) mixtures of graphitic and non-graphitic carbon in association with minerals.

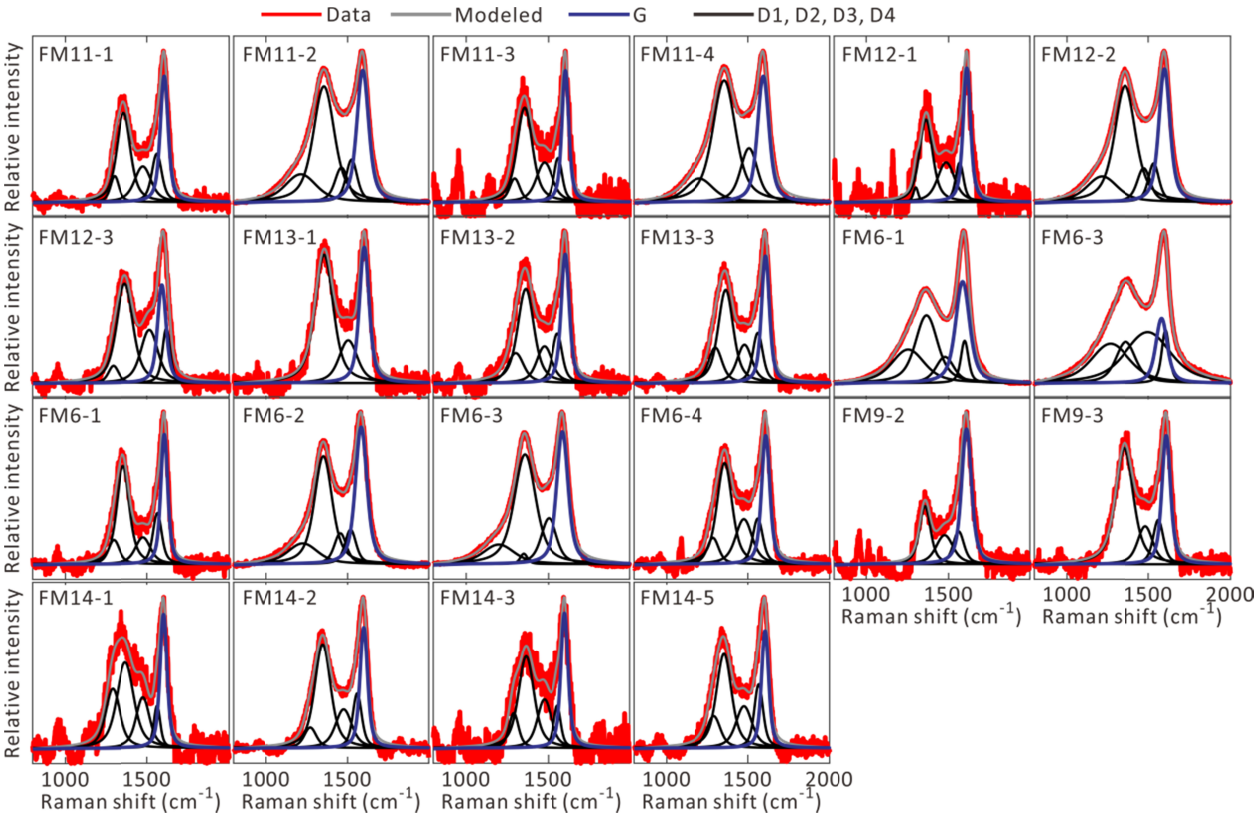

Figure S3. Baseline-corrected Raman spectra of the CJ fly ash samples decomposed to G and D1-D4 bands by fitting Lorentzian profiles to five Raman peaks following Sparkes et al. (6). Only those Raman spectra returning stable fitting results are reported.

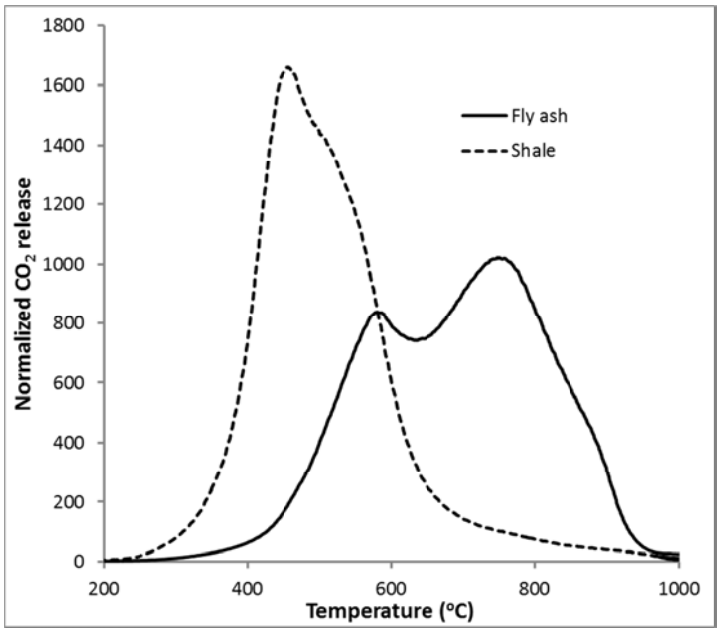

Figure S4. Thermograms of the CJ fly ash sample (FM8) and the shale sample (NJBS4-2) obtained from RPO analysis.

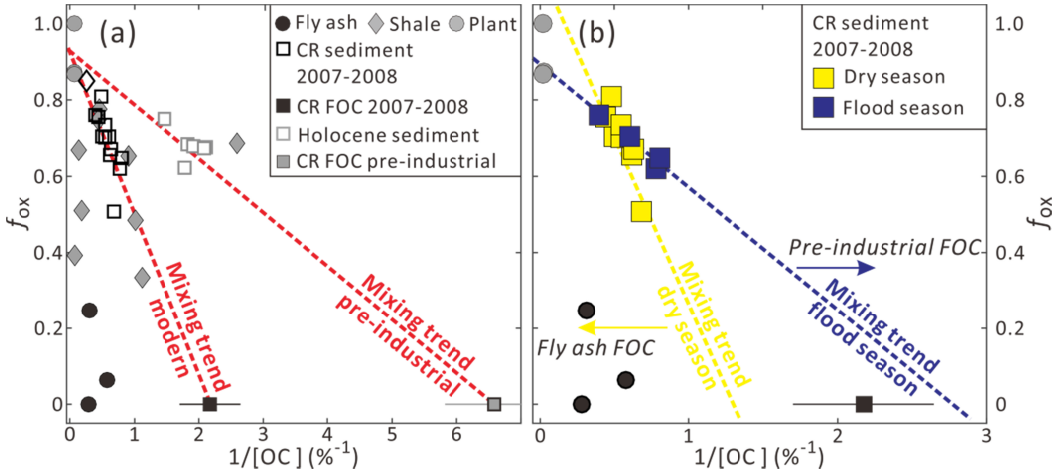

Figure S5. (a) Oxidation fraction (f_{ox}) versus 1/OC for all studied samples, with the two dashed lines show the mixing trends between fossil OC and biospheric OC end-members for modern-day river sediment samples and for pre-industrial, Holocene core sediment samples. (b) Oxidation fraction (f_{ox}) versus 1/OC for the collected Chang Jiang suspended sediment samples, and plant and fly ash samples. The CJ sediment samples are grouped by those collected in the flood season (blue) versus in the dry season (yellow) (2), and the two mixing trends (dashed lines) are determined from linear regression of each sample group.

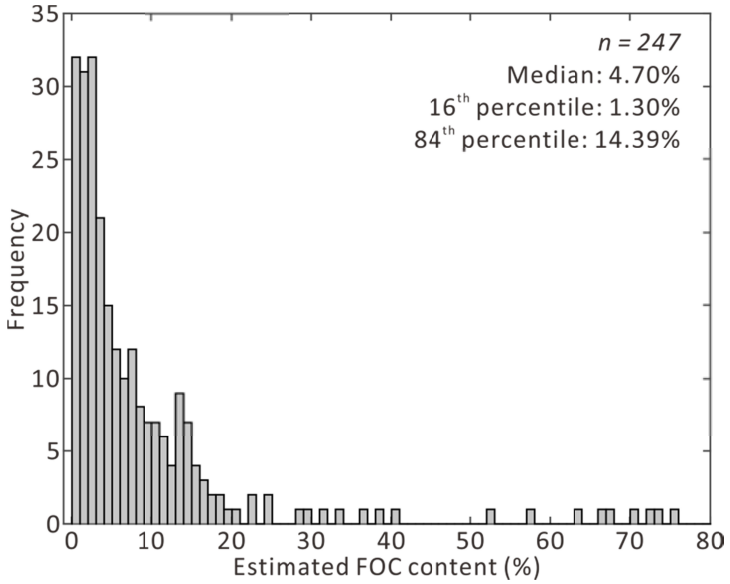

Figure S6. Histogram of compiled FOC content estimated by multiple approaches (LOI and elemental analysis) in global fly ash samples (raw data and details in Table S2).

Supporting Information Appendix Tables (Uploaded as separated spreadsheets)

Table S1. Sample information, OC content, and oxidation fraction

Table S2. Compilation of fly ash OC content estimates for global fly ash samples

References

1. Yang SY, *et al.* (2011) Burial of organic carbon in Holocene sediments of the Zhujiang (Pearl River) and Changjiang (Yangtze River) estuaries. *Marine Chemistry* 123(1-4):1-10.
2. Li G, *et al.* (2015) Dam-triggered organic carbon sequestration makes the Changjiang (Yangtze) river basin (China) a significant carbon sink. *Journal of Geophysical Research: Biogeosciences* 120(1):2014JG002646.
3. Clark KE, *et al.* (2013) New views on 'old' carbon in the Amazon river: Insight from the source of organic carbon eroded from the Peruvian Andes. *Geochemistry, Geophysics, Geosystems*:1644-1659.
4. Helfrich M, Flessa H, Mikutta R, Dreves A, & Ludwig B (2007) Comparison of chemical fractionation methods for isolating stable soil organic carbon pools. *Eur J Soil Sci* 58(6):1316-1329.
5. Galy V, Beyssac O, France-Lanord C, & Eglinton T (2008) Recycling of graphite during Himalayan erosion: a geological stabilization of carbon in the crust. *Science* 322.
6. Sparkes R, Hovius N, Galy A, Kumar RV, & Liu JT (2013) Automated Analysis of Carbon in Powdered Geological and Environmental Samples by Raman Spectroscopy. *Applied spectroscopy* 67(7):779-788.
7. Hemingway JD (2019) Mineral protection regulates long-term global preservation of natural organic carbon. *Nature* 570.
8. Hemingway JD, Rothman DH, Rosengard SZ, & Galy VV (2017) Technical note: An inverse method to relate organic carbon reactivity to isotope composition from serial oxidation. *Biogeosciences* 14(22):5099-5114.
9. Rosenheim BE & Galy V (2012) Direct measurement of riverine particulate organic carbon

age structure. *Geophysical Research Letters* 39(19).
10. National Bureau of Statistics of China (2009) China Statistical Yearbook.
11. National Bureau of Statistics of China (2012) China Statistical Yearbook.
12. Yao ZT, *et al.* (2015) A comprehensive review on the applications of coal fly ash. *Earth-Science Reviews* 141:105-121.
13. National Development and Reform Commission of China (2012) *Annual Report on Comprehensive Utilization of Resources of China*. http://www.gov.cn/gzdt/2013-04/08/content_2372577.htm.
14. National Bureau of Statistics of China (2012) *China Energy Statistical Yearbook*.
15. Chang Jiang Water Commission (2009) Chang Jiang sediment bulletin.
16. Chen XQ, Yan YX, Fu RS, Dou XP, & Zhang EF (2008) Sediment transport from the Yangtze River, China, into the sea over the Post-Three Gorge Dam Period: A discussion. *Quaternary International* 186:55-64.
17. Global Energy Monitor (2019) Global Coal Plant Tracker. https://endcoal.org/global-coal-plant-tracker/
18. Center for Global Development (2012) Carbon Dioxide Emissions From Power Plants Worldwide (CARMA). https://www.cgdev.org/article/carma-v30-reveals-new-data-co2-emissions-corporate-ownership-and-locations-60000-power
19. Yang SL, *et al.* (2005) Impact of dams on Yangtze River sediment supply to the sea and delta intertidal wetland response. *J Geophys Res-Earth* 110(F3).
20. Inland Water Biological Division of Chinese Biodiversity Information Center (2012) Database of the Basic Characteristics of Chinese Large and Medium-Scale Reservoirs. https://web.archive.org/web/20120330041630/http://brim.ihb.ac.cn/indexen.aspx
21. Ministry of Water Resources of China (2011) Code for China Reservoir Name.
22. Galy V (2007) Efficient organic carbon burial in the Bengal fan sustained by the Himalayan erosional system. *Nature* 450.
23. Blair NE & Aller RC (2012) The fate of terrestrial organic carbon in the marine environment. *Annu. Rev. Mar. Sci.* 4.
24. Bouchez J, *et al.* (2010) Oxidation of petrogenic organic carbon in the Amazon floodplain as a source of atmospheric CO_2. *Geology* 38(3):255-258.
25. Hemingway JD (2018) Microbial oxidation of lithospheric organic carbon in rapidly eroding tropical mountain soils. *Science* 360.
26. Hilton RG, Gaillardet JÔ, Calmels D, & Birck JL (2014) Geological respiration of a mountain belt revealed by the trace element rhenium. *Earth Planet. Sci. Lett.* 403.
27. Chang Jiang Water Commission (2008) Chang Jiang Sediment Bulletin.
28. Li FL, Li GJ, & Ji JF (2011) Increasing magnetic susceptibility of the suspended particles in Yangtze River and possible contribution of fly ash. *Catena* 87(1):141-146.
29. Li M, *et al.* (2018) Role of elemental carbon in the photochemical aging of soot. *Proceedings of the National Academy of Sciences* 115(30):7717-7722.
30. Andersen ME, *et al.* (2017) Soot, organics, and ultrafine ash from air- and oxy-fired coal combustion. *Proceedings of the Combustion Institute* 36(3):4029-4037.
31. Sotch A (2015) Fly ash from coal combustion - characterization. Master (Técnico Lisboa, Lisboa).

32. Dindarloo SR & Hower JC (2015) Prediction of the unburned carbon content of fly ash in coal-fired power plants. *Coal Combustion and Gasification Products* 7:19-29.
33. Argiz C, Menéndez E, Moragues A, & Sanjuán MA (2015) Fly ash characteristics of Spanish coal-fired power plants. *Afinidad* 72(572).
34. Dong NS (2010) *Reducing Carbon-in-Ash* (IEA Clean Coal Centre) p 65.
35. Xing Y*, et al.* (2019) Separation of unburned carbon from coal fly ash: A review. *Powder Technology* 353:372-384.
36. Stanmore BR, Brilhac JF, & Gilot P (2001) The oxidation of soot: a review of experiments, mechanisms and models. *Carbon* 39(15):2247-2268.
37. Hower JC*, et al.* (2017) Coal-derived unburned carbons in fly ash: A review. *International Journal of Coal Geology* 179:11-27.
38. Bhatt A*, et al.* (2019) Physical, chemical, and geotechnical properties of coal fly ash: A global review. *Case Studies in Construction Materials* 11:e00263.
39. Ahmaruzzaman M (2010) A review on the utilization of fly ash. *Progress in Energy and Combustion Science* 36(3):327-363.
40. Hao Z, Qian X, Cen K, & Jianren F (2004) Optimizing pulverized coal combustion performance based on ANN and GA. *Fuel Processing Technology* 85(2):113-124.
41. Bartoňová L (2015) Unburned carbon from coal combustion ash: An overview. *Fuel Processing Technology* 134:136-158.
42. Gao Y-M, Shim H-S, Hurt RH, Suuberg EM, & Yang NYC (1997) Effects of Carbon on Air Entrainment in Fly Ash Concrete: The Role of Soot and Carbon Black. *Energy & Fuels* 11(2):457-462.
43. ASTM International (2015) ASTM C618-15. Standard specification for coal fly ash and raw or calcined natural pozzolan for use in concrete. (West Conshohocken, PA).
44. Jha CN & Prasad JK (2009) *A resource material for innovative building material - Indian perspective* (New Delhi, India), (Poverty MoUE).
45. Standards Australia International (1998) Austrailian Standard AS3582.1. Supplementary cementitious materials for use with Portland and Blended cement - Part 1: fly ash. in *(ISBN 0733716881)*.
46. Putilov VY & Putilova IV (2005) Modern approach to the problem of utilization of fly ash and bottom ash from power plants in Russia. in *2005 Word of Coal Ash (WOCA)* (Lexington, Kentucky, USA).
47. Kutchko BG & Kim AG (2006) Fly ash characterization by SEM–EDS. *Fuel* 85(17):2537-2544.
48. Surabhi, Udayabhanu G, & Suresh N (2006) Characterization of Unburnt Carbon Recovered from Fly Ash by Froth Flotation. *Proceedings of the International Seminar on Mineral Processing Technology and Indo-Korean Workshop on Resource Recycling (MPT-2006)*.
49. Hower JC, Graham UM, Dozier A, Tseng MT, & Khatri RA (2008) Association of the Sites of Heavy Metals with Nanoscale Carbon in a Kentucky Electrostatic Precipitator Fly Ash. *Environmental Science & Technology* 42(22):8471-8477.
50. Külaots I, Hurt RH, & Suuberg EM (2004) Size distribution of unburned carbon in coal fly ash and its implications. *Fuel* 83(2):223-230.
51. Burdige DJ (2007) Preservation of organic matter in marine sediments: controls, mechanisms, and an imbalance in sediment organic carbon budgets? *Chem. Rev.* 107.

52. Badenhorst CJ*, et al.* (2019) Separation of unburned carbon from coal conversion ash: Development and assessment of a dry method. *Coal combustion and gasification products* 11(2):89-96.
53. Rubio B, Izquierdo MT, Mayoral MC, Bona MT, & Martínez-Tarazona RM (2008) Preparation and characterization of carbon-enriched coal fly ash. *Journal of Environmental Management* 88(4):1562-1570.
54. Hwang J, Sun X, & Li Z (2002) Unburned carbon from fly ash for mercury adsorption: I. separation and characterization of unburned carbon. *Journal of Minerals and Materials Characterization and Engineering* 1(1):39-60.
55. Blissett RS & Rowson NA (2012) A review of the multi-component utilisation of coal fly ash. *Fuel* 97:1-23.
56. Bittner JD, Hrach FJ, Gasiorowski SA, Canellopoulus LA, & Guicherd H (2014) Triboelectric Belt Separator for Beneficiation of Fine Minerals. *Procedia Engineering* 83:122-129.
57. Cangialosi F, Notarnicola M, Liberti L, & Stencel J (2009) The role of weathering on fly ash charge distribution during triboelectrostatic beneficiation. *Journal of Hazardous Materials* 164(2):683-688.
58. Xia Y, Yang Z, Zhang R, Xing Y, & Gui X (2019) Enhancement of the surface hydrophobicity of low-rank coal by adsorbing DTAB: An experimental and molecular dynamics simulation study. *Fuel* 239:145-152.
59. Ramaswamy B, Kar DD, & De S (2007) A study on recovery of oil from sludge containing oil using froth flotation. *Journal of Environmental Management* 85(1):150-154.
60. Rao SR (2004) *Surface Chemistry of Froth Flotation Volume 1: Fundamentals* (Springer, Boston, MA).
61. Huang Y, Takaoka M, & Takeda N (2003) Removal of unburned carbon from municipal solid waste fly ash by column flotation. *Waste Management* 23(4):307-313.
62. Walker A & Wheelock TD (2006) Separation of Carbon from Fly Ash Using Froth Flotation. *Coal Preparation* 26(4):235-250.
63. Eisele TC & Kawatra SK (2002) Use of froth flotation to remove unburned carbon from fly ash. *Mineral Processing and Extractive Metallurgy Review* 23(1):1-10.
64. Zhang W & Honaker R (2015) Studies on carbon flotation from fly ash. *Fuel Processing Technology* 139:236-241.
65. Şahbaz O, Öteyaka B, Kelebek Ş, Uçar A, & Demir U (2008) Separation of unburned carbonaceous matter in bottom ash using Jameson cell. *Separation and Purification Technology* 62(1):103-109.
66. Emre Altun N, Xiao C, & Hwang J-Y (2009) Separation of unburned carbon from fly ash using a concurrent flotation column. *Fuel Processing Technology* 90(12):1464-1470.
67. Zhang H*, et al.* (2013) Cyclonic-static micro-bubble flotation column. *Minerals Engineering* 45:1-3.
68. Huang TY, Chiueh PT, & Lo SL (2017) Life-cycle environmental and cost impacts of reusing fly ash. *Resources, Conservation and Recycling* 123:255-260.
69. Gray ML, Champagne KJ, Soong Y, & Finseth DH (2001) Parametric study of the column oil agglomeration of fly ash. *Fuel* 80(6):867-871.
70. Long CM, Nascarella MA, & Valberg PA (2013) Carbon black vs. black carbon and other

airborne materials containing elemental carbon: Physical and chemical distinctions. *Environmental Pollution* 181:271-286.
71. Bartoňová L, Juchelková D, Klika Z, & Cech B (2011) On unburned carbon in coal ash from various combustion units. *International Journal of Materials and Metallurgical Engineering* 5(4):302-305.
72. Dai S, *et al.* (2010) Abundances and distribution of minerals and elements in high-alumina coal fly ash from the Jungar Power Plant, Inner Mongolia, China. *International Journal of Coal Geology* 81(4):320-332.
73. Liu J, Dai S, He X, Hower JC, & Sakulpitakphon T (2017) Size-Dependent Variations in Fly Ash Trace Element Chemistry: Examples from a Kentucky Power Plant and with Emphasis on Rare Earth Elements. *Energy & Fuels* 31(1):438-447.
74. Heidrich C, Feuerborn H-J, & Weir A (2013) Coal combustion products: A global perspective. in *2013 World of Coal Ash (WOCA) Conference* (Lexington, KY).
75. Dai S, *et al.* (2014) Composition and modes of occurrence of minerals and elements in coal combustion products derived from high-Ge coals. *International Journal of Coal Geology* 121:79-97.
76. Shibaoka M (1985) Microscopic investigation of unburnt char in fly ash. *Fuel* 64(2):263-269.
77. Vleeskens JM, Menéndez RM, Roos CM, & Thomas CG (1993) Combustion in the burnout stage: the fate of inertinite. *Fuel Processing Technology* 36(1):91-99.
78. Goodarzi F & Hower JC (2008) Classification of carbon in Canadian fly ashes and their implications in the capture of mercury. *Fuel* 87(10):1949-1957.
79. Kostova I, Vassileva C, Dai S, Hower JC, & Apostolova D (2013) Influence of surface area properties on mercury capture behaviour of coal fly ashes from some Bulgarian power plants. *International Journal of Coal Geology* 116-117:227-235.
80. Hower JC & Mastalerz M (2001) An Approach toward a Combined Scheme for the Petrographic Classification of Fly Ash. *Energy & Fuels* 15(5):1319-1321.
81. Maroto-Valer MM, Taulbee DN, & Hower JC (2001) Characterization of differing forms of unburned carbon present in fly ash separated by density gradient centrifugation. *Fuel* 80(6):795-800.
82. Wilcox J, *et al.* (2015) Observations and Assessment of Fly Ashes from High-Sulfur Bituminous Coals and Blends of High-Sulfur Bituminous and Subbituminous Coals: Environmental Processes Recorded at the Macro- and Nanometer Scale. *Energy & Fuels* 29(11):7168-7177.
83. Chen Y, Shah N, Huggins FE, & Huffman GP (2006) Microanalysis of ambient particles from Lexington, KY, by electron microscopy. *Atmospheric Environment* 40(4):651-663.
84. Linak WP, *et al.* (2007) Ultrafine ash aerosols from coal combustion: Characterization and health effects. *Proceedings of the Combustion Institute* 31(2):1929-1937.
85. Silva LFO, *et al.* (2012) Applied investigation on the interaction of hazardous elements binding on ultrafine and nanoparticles in Chinese anthracite-derived fly ash. *Science of The Total Environment* 419:250-264.
86. Hower JC, Hood MM, Taggart RK, & Hsu-Kim H (2017) Chemistry and petrology of paired feed coal and combustion ash from anthracite-burning stoker boilers. *Fuel* 199:438-446.
87. Baltrus JP, Wells AW, Fauth DJ, Diehl JR, & White CM (2001) Characterization of Carbon Concentrates from Coal-Combustion Fly Ash. *Energy & Fuels* 15(2):455-462.

88. Bartoňová L, Klika Z, & Spears DA (2007) Characterization of unburned carbon from ash after bituminous coal and lignite combustion in CFBs. *Fuel* 86(3):455-463.
89. Brown RC & Dykstra J (1995) Systematic errors in the use of loss-on-ignition to measure unburned carbon in fly ash. *Fuel* 74(4):570-574.
90. Fan M & Brown RC (2001) Comparison of the Loss-on-Ignition and Thermogravimetric Analysis Techniques in Measuring Unburned Carbon in Coal Fly Ash. *Energy & Fuels* 15(6):1414-1417.
91. Ha T-H*, et al.* (2005) Effect of unburnt carbon on the corrosion performance of fly ash cement mortar. *Construction and Building Materials* 19(7):509-515.
92. Hower JC, Sakulpitakphon T, Trimble AS, Thomas GA, & Schram WH (2006) Major and Minor Element Distribution in Fly Ash from a Coal-Fired Utility Boiler in Kentucky. *Energy Sources, Part A: Recovery, Utilization, and Environmental Effects* 28(1):79-95.
93. Mardon SM & Hower JC (2004) Impact of coal properties on coal combustion by-product quality: examples from a Kentucky power plant. *International Journal of Coal Geology* 59(3):153-169.
94. Mohebbi M, Rajabipour F, & Scheetz BE (2017) Evaluation of Two-Atmosphere Thermogravimetric Analysis for Determining the Unburned Carbon Content in Fly Ash. *Advances in Civil Engineering Materials* 6(1):258-279.
95. Payá J, Monzó J, Borrachero MV, Perris E, & Amahjour F (1998) Thermogravimetric Methods for Determining Carbon Content in Fly Ashes. *Cement and Concrete Research* 28(5):675-686.
96. Wang S & Zhu ZH (2007) Humic acid adsorption on fly ash and its derived unburned carbon. *Journal of Colloid and Interface Science* 315(1):41-46.
97. ASTM International (2013) ASTM D7348-13. Standard test methods for loss on ignition (LOI) of solid combustion residues (West Conshohocken, PA).